PROCEEDINGS A

royalsocietypublishing.org/journal/rspa

Research

Cite this article: Mukherjee S, Dhar J, DasGupta S, Chakraborty S. 2019 Patterned surface charges coupled with thermal gradients may create giant augmentations of solute dispersion in electro-osmosis of viscoelastic fluids. *Proc. R. Soc. A* **475**: 20180522.
http://dx.doi.org/10.1098/rspa.2018.0522

Received: 2 August 2018
Accepted: 29 November 2018

Subject Areas:
fluid mechanics

Keywords:
dispersion, electrothermal effect, viscoelastic fluid

Author for correspondence:
Suman Chakraborty
e-mail: suman@mech.iitkgp.ernet.in

Downloaded from https://royalsocietypublishing.org/ on 30 January 2023

Patterned surface charges coupled with thermal gradients may create giant augmentations of solute dispersion in electro-osmosis of viscoelastic fluids

Siddhartha Mukherjee[1], Jayabrata Dhar[2], Sunando DasGupta[1,3] and Suman Chakraborty[1,2]

[1]Advanced Technology Development Center, [2]Department of Mechanical Engineering, and [3]Department of Chemical Engineering, Indian Institute of Technology Kharagpur, Kharagpur 721302, India

JD, 0000-0002-7487-4929; SC, 0000-0002-5454-9766

Augmenting the dispersion of a solute species and fluidic mixing remains a challenging proposition in electrically actuated microfluidic devices, primarily due to an inherent plug-like nature of the velocity profile under uniform surface charge conditions. While a judicious patterning of surface charges may obviate some of the concerning challenges, the consequent improvement in solute dispersion may turn out to be marginal. Here, we show that by exploiting a unique coupling of patterned surface charges with intrinsically induced thermal gradients, it may be possible to realize giant augmentations in solute dispersion in electro-osmotic flows. This is effectively mediated by the phenomena of Joule heating and surface heat dissipation, so as to induce local variations in electrical properties. Combined with the rheological premises of a viscoelastic fluid that are typically reminiscent of common biofluids handled in lab-on-a-chip-based micro-devices, our results demonstrate that the consequent electro-hydrodynamic forcing may open up favourable windows for augmented hydrodynamic dispersion, which has not yet been unveiled.

Electronic supplementary material is available online at https://dx.doi.org/10.6084/m9.figshare.c.4337252.

THE ROYAL SOCIETY PUBLISHING

© 2019 The Author(s) Published by the Royal Society. All rights reserved.

Downloaded from https://royalsocietypublishing.org/ on 30 January 2023

1. Introduction

Miniaturization of fluidic devices has attracted significant research attention in recent years [1,2]. With further advancements in understanding the underlying science, newer control techniques have been explored with a vision to achieve augmented mixing [3–8] or separation [9–11], consistent with the demands of specific applications. Towards achieving quality mixing in miniaturized devices, the phenomena of diffusion and dispersion stand as the two advantageous mechanisms [12,13]. Hydrodynamic dispersion is a process in which band broadening of a neutral solute occurs because of non-uniformity in the velocity distribution [14–18]. Controlling hydrodynamic dispersion necessarily holds a key towards realizing optimal functionalities of several microfluidic devices of contemporary relevance [19–25].

Typical miniaturized devices in the modern day lab-on-a-chip environment handle biological fluids that tend to disobey Newton's law of viscosity [26–31]. In particular, biofluids, like blood plasma, saliva, synovial fluid and vitreous humour [32–36], exhibit viscoelasticity under certain straining conditions. Hence, the use of viscoelastic models to predict their dynamical features remains pertinent [37–42]. Accordingly, hydrodynamic dispersion characteristics of viscoelastic fluids have emerged as an important research topic over the recent years.

Furthermore, hydrodynamic dispersion in electrokinetic transport turns out to be of significant consequence, because of its wide spectrum of relevance ranging from medical diagnostics [43–46] to power production and thermal management of micro-devices [2,47–51]. In sharp contrast to pressure-driven flow, electro-osmotic flow (EOF) typically exhibits plug-type velocity profile when the electrical double layer (EDL) thickness is small when compared with the channel dimension, provided that the surface charge distribution is spatially uniform [52,53]. Despite having many other advantages, this uniformity in the velocity profile of the EOF results in decline of mixing performance and solute dispersion in comparison to pressure-driven flow. Thus, to improve the extent of mixing, the usual approach is to bring non-uniformity in the channel geometry or to alter the surface charge distribution [54,55], thereby bringing out circulatory patterns in the flow field [56,57]. Such surface charge modulation, in principle, can be used in conjunction with other effects such as electrothermal flow [58], thin film patterning [59], AC electro-osmosis [60–63] and induced-charge electro-osmosis [64]. In parallel, electrokinetically driven flows of viscoelastic fluids have also drawn special attention because of their emerging applications ranging from species separation [65,66] to energy conversion in microfluidic devices [67,68].

Previous research has established the fact that the interplay between the temperature and concentration over small length scales may be exploited to further enhance solute dispersion in a medium [69,70]. Temperature gradients may occur either due to intrinsic Joule heating or via an external heat source [78–84]. The developed non-isothermal condition results in the variation of the physical properties like viscosity, permittivity, electrical and thermal conductivity. For instance, the variation in the fluid conductivity interacting with the electric field can be used as a flow actuation mechanism, commonly termed as electro-convection. Such temperature dependence of the physical properties may result in drastic alteration in the flow field. Besides, the materials widely used for microchannel fabrication, like polymethylmethacrylate (PMMA) and polydimethylsiloxane (PDMS), have lower specific heat capacities, and the lesser dissipation of heat from these materials may further contribute to augment the local temperature gradients, thus affecting the flow physics. While several studies have been directed towards the efficient transportation of fluid using the temperature-dependent property variations, the contribution of the electro-thermal perturbation to the coupled electro-hydrodynamic solute transport remains unexplored. More specifically, the combined consequences of electro-thermal interaction and fluid rheology, along with surface charge modulation, may give rise to interesting implications in solute dispersion, which remains to be investigated. For amplification of the dispersion coefficient, a number of research works have been devoted by introducing non-uniformity in the flow domain, for example using variable electric field, non-uniform zeta potential distribution, different types of electrolytes and axial variation in cross-section, several studies have been

Downloaded from https://royalsocietypublishing.org/ on 30 January 2023

directed towards augmenting the hydrodynamic dispersion [19,20,75–79]. However, as discussed earlier, the intrinsically induced temperature gradient in narrow confinement due to Joule heating can play a pivotal role in governing the flow physics by inducing more pressure distribution which, in turn, strongly influences the associated hydrodynamic dispersion.

In this context, we delineate the effect of electro-thermal perturbations on the hydrodynamic dispersion of a viscoelastic fluid flowing through a parallel plate microchannel having modulated interfacial charges, under surface and volumetric heat transfer. We show that the physical property variations owing to the prevailing temperature distribution, coupled with the surface charge modulation, may result in giant augmentation of hydrodynamic dispersion, for typical viscoelastic fluids considered in this work. These results may open up new paradigms of massively augmented solute dispersion in lab-on-a-chip devices handling biological fluids, by extending other relevant works in this field [61–63].

2. Problem formulation

Figure 1 depicts the schematic of a parallel plate microchannel subjected to a convective heat loss, in conjunction with patterned surface charges (equivalently, patterned surface potential). The half-width of the microchannel is denoted by h, which is much smaller when compared with the length (l) of the microchannel, i.e. $h \ll l$. The longitudinal and transverse coordinates are chosen along and perpendicular to the flow direction, respectively, with the centreline at the inlet being the origin of the coordinate system, as depicted in the figure. To implement the patterned surface condition, we have chosen the following axial variation of the zeta potential: $\zeta = \zeta_{\text{ref}}\{\alpha_1 + \alpha_2 \cos(\omega_t x)\}$, induced at the fluid–surface interface. Here, ζ_{ref} is the reference zeta potential, α_1 and α_2 are the axially invariant and patterned contributions of the modulated zeta potential, while ω_t is the patterning frequency. Both ends of the microchannel are maintained at constant temperature (T_{ref}) and pressure (p_{atm}). An external electric potential is considered to be applied in the axial direction. The heat generated due to the Joule heating effect is dissipated to the surrounding through surface convection. Before presenting the governing equations for the above system, it is necessary to discuss all the assumptions required for this analysis.

In this study, we consider a symmetric binary electrolyte (z: z) being subjected to externally applied electric potential and transverse equilibrium distribution of charges due to the EDL phenomenon. The flow is assumed to be steady, laminar, incompressible and in the creeping flow regime, i.e. $Re \ll 1$. The physical properties of the fluid like viscosity (μ_{eff}), thermal conductivity (k_{eff}), electrical conductivity (σ_{eff}), electrical permittivity (ε_{eff}) and relaxation time (λ_{eff}) are considered to be temperature-dependent. We further assume that the free ionic species within the EDL are point charges and they are in local equilibrium. Under this assumption, the advection term in the Poisson–Nernst–Plank equation can be safely neglected and the Poisson–Boltzmann description of the charge distribution remains valid [54,55] (rationale behind this consideration is discussed in electronic supplementary material, section A1). For low values of zeta potential (ζ) (i.e. $\zeta < 25$ mV), the well-known Debye–Hückel linearization approximation for the potential distribution can be applied [55,57]. Finally, we assume that the weak electric field (E_{ref}) approximation is valid, i.e. $E_{\text{ref}} \ll \zeta_{\text{ref}}/\lambda_D$, where λ_{D} is the Debye length, very small when compared to the channel dimension (h) thus precluding any distortion of the EDL structure [1,56]. After taking into account the foregoing assumptions, the continuity, momentum and energy equations take the following form:

$$\left.\begin{aligned} \nabla \cdot \boldsymbol{v} &= 0 \\ \rho(\boldsymbol{v} \cdot \nabla)\boldsymbol{v} &= -\nabla p + \nabla \cdot \boldsymbol{\tau} + \boldsymbol{F_b} \\ \rho\, C_p(\boldsymbol{v} \cdot \nabla T) &= \nabla \cdot (k_{\text{eff}} \nabla T) + Q_{\text{gen}} + Q_{\text{vd}} \end{aligned}\right\}, \tag{2.1}$$

where $\boldsymbol{v}$ is the velocity vector, $\boldsymbol{\tau}$ is the stress tensor, p is the hydrodynamic pressure and T is the temperature field. ρ and C_p are the density and specific heat capacities of the fluid, respectively. k_{eff} is the thermal conductivity of the fluid obeying the following relationship

Downloaded from https://royalsocietypublishing.org/ on 30 January 2023

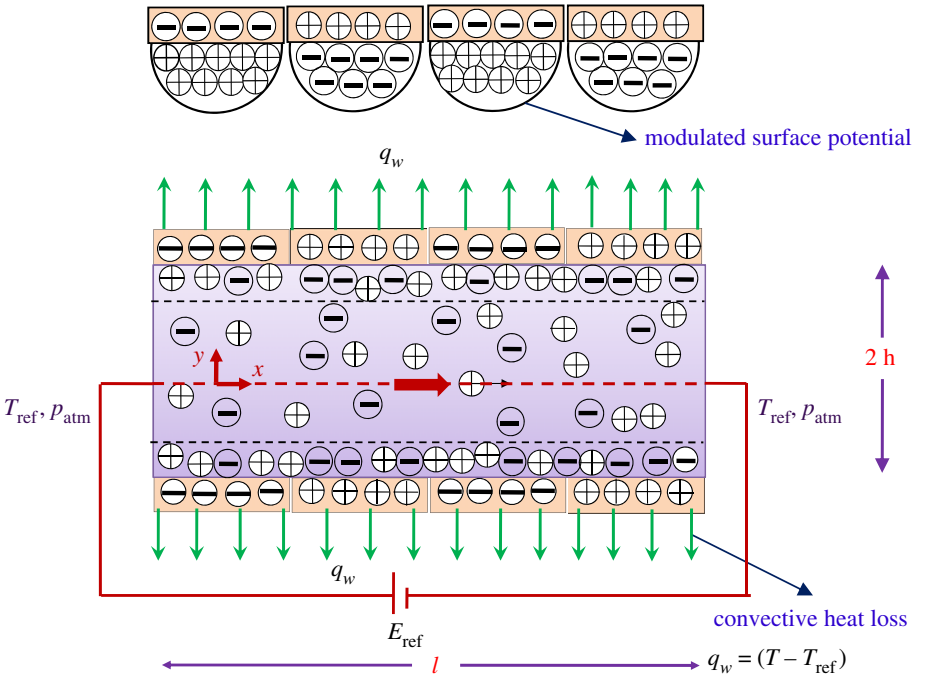

Figure 1. Schematic depiction of the physical problem. (Online version in colour.)

$k_{eff} = k_{ref}[1 + \alpha_3(T - T_{ref})]$, where k_{ref} is the reference thermal conductivity evaluated at reference temperature T_{ref} with α_3 being the temperature sensitivity of thermal conductivity. In the momentum equation, $\boldsymbol{F_b}$ is the electrokinetic body force defined by $\boldsymbol{F_b} = \rho_e \boldsymbol{E} - |\boldsymbol{E}|^2 \nabla \varepsilon_{eff}/2 + \nabla\{\rho(\partial\varepsilon/\partial\rho)_T |\boldsymbol{E}|^2\}$, where ρ_e is the free charge density and $\boldsymbol{E}$ is the electric field written as $\boldsymbol{E} = -\nabla\Phi$ with Φ being the electric potential. The three terms in the body force are the Columbic force, dielectrophoretic force and electrostriction forces. The Columbic force is induced due to the presence of free space charges and the variation in the electrical permittivity gives rise to the dielectrophoretic force, while the electrostriction force represents the compressibility of the fluid medium and thus can be neglected for incompressible fluids. In the energy equation, Q_{gen} is the heat generated due to the Joule heating effect, $Q_{gen} = \sigma_{eff}|\boldsymbol{E}|^2$ and Q_{vd} is the heat dissipation due to viscous action. σ_{eff} and ε_{eff} are the electrical conductivity and permittivity of the fluid, respectively, which depend on temperature in the following way: $\sigma_{eff} = \sigma_{ref}[1 + \alpha_4(T - T_{ref})]$ and $\varepsilon_{eff} = \varepsilon_{ref}[1 - \alpha_5(T - T_{ref})]$. Here, σ_{ref} and ε_{ref} are the reference values of electrical conductivity and permittivity of fluid at T_{ref} with α_4 and α_5 being their temperature sensitivities, respectively [83]. To determine the electric field, we make use of the charge distribution equation along with the current continuity equation given by the following equation:

$$\left.\begin{aligned} \nabla \cdot (\varepsilon_{eff} \nabla \Phi) &= -\rho_e \\ \nabla \cdot \boldsymbol{i} = \nabla \cdot (\sigma_{eff} \boldsymbol{E} + \boldsymbol{v}\, q - D\, \nabla q) &= 0 \end{aligned}\right\}. \tag{2.2}$$

The charge distribution subjected to the assumption of the Poisson–Boltzmann description yields $\nabla \cdot (\varepsilon_{eff} \nabla \Phi) = -\rho_e = 2\, n_0\, z\, e\ \sinh\{z\, e\, \Phi / k_B\, T\}$, where n_0 is the number density of ions, k_B Boltzmann constant, z valence of ions, e electronic charge and T absolute temperature. In the current continuity equation, $q = -\rho_e$ and D is the diffusion coefficient. The current continuity equation consists of three components: the first term represents the Ohmic contribution part due to the conduction of charges, while the second and third terms are advective and diffusive components, respectively. In this analysis, the advective and diffusive components are neglected with respect to the Ohmic contribution. This is possible only under the assumption of a thin

Downloaded from https://royalsocietypublishing.org/ on 30 January 2023

EDL [10,64,84], which implies that the region of electro-neutrality (i.e. the region of vanishing charge density) is considerably larger when compared with the EDL region. Considering this, the electric potential becomes essentially the sum of two potentials, one that prevails outside the EDL ($\phi(x)$), another one that is induced within the EDL $\psi(x, y)$, i.e. $\Phi(x, y) = \phi(x) + \psi(x, y)$. Using this consideration, the Poisson–Boltzmann equation and the current continuity equation become

$$\left.\begin{aligned} &\frac{\partial}{\partial x}\left\{\varepsilon_{\mathrm{eff}}\left(\frac{\mathrm{d}\phi}{\mathrm{d}x}+\frac{\partial\psi}{\partial x}\right)\right\}+\frac{\partial}{\partial y}\left\{\varepsilon_{\mathrm{eff}}\left(\frac{\partial\psi}{\partial y}\right)\right\}=2n_0 z e \sinh\left(\frac{z e\psi}{k_{\mathrm{B}}T}\right)\\ &\frac{\partial}{\partial x}\left\{\sigma_{\mathrm{eff}}\left(\frac{\mathrm{d}\phi}{\mathrm{d}x}+\frac{\partial\psi}{\partial x}\right)\right\}+\frac{\partial}{\partial y}\left\{\sigma_{\mathrm{eff}}\left(\frac{\partial\psi}{\partial y}\right)\right\}=0 \end{aligned}\right\}. \tag{2.3}$$

Employing the Debye–Hückel linearization, we have $\sinh\{z e\psi/(k_{\mathrm{B}}T)\} \approx z e\psi/(k_{\mathrm{B}}T)$. Thus, the Poisson–Boltzmann equation recasts as $\nabla\cdot(\varepsilon_{\mathrm{eff}}\nabla\Phi) = 2n_0 z^2 e^2\psi/(k_{\mathrm{B}}T)$. Next, we compare the contribution of two components of the current continuity equation: $i_x \sim \sigma_{\mathrm{ref}}E_{\mathrm{ref}}$ and $i_y \sim \sigma_{\mathrm{ref}}\zeta_{\mathrm{ref}}/2h$, which gives $i_x/i_y \gg 1$, and the simplified equation is now integrated across the channel dimension:

$$\int_{-h}^{h}\frac{\partial}{\partial x}\left\{\sigma_{\mathrm{eff}}\left(\frac{\mathrm{d}\phi}{\mathrm{d}x}+\frac{\partial\psi}{\partial x}\right)\right\}\mathrm{d}y = 0. \tag{2.4}$$

In the energy equation, one can neglect the relative contribution of the viscous dissipation term (Q_{vd}) with respect to the conduction and heat generation (due to Joule heating) terms. This can be done by performing a scaling analysis of the relative strength between these terms. To obtain this, we here introduce a new variable Ω which is the ratio of the strength of viscous dissipation to the heat generation due to Joule heating (this is analogous to the Brinkman number (Br), which is basically the ratio of viscous dissipation to the imposed wall heat flux, typically used in forced convective heat transfer problems). Here, choosing appropriate scales of the parameters, Ω is found to be $\Omega \sim \mu_{\mathrm{ref}}{u_c}^2/\sigma_{\mathrm{ref}}E^2h^2$, where the typical values of the parameters are as follows: $\mu_{\mathrm{ref}} \sim 10^{-3}$ Pa s, $u_c = u_{\mathrm{HS}} \sim 10^{-3}\,\mathrm{m\,s^{-1}}$, $\sigma_{\mathrm{ref}} \sim 10^{-2} - 10^{-1}\,\mathrm{S\,m^{-1}}$ and $E_{\mathrm{ref}} \sim 10^3 - 10^4\,\mathrm{V\,m^{-1}}$. Here, the channel height is chosen to be of the order of ~10–100 µm, while in electrokinetic studies the EDL thickness is usually of ~1–10 nm and, hence, thin EDL assumption can be safely taken into consideration. Hence, the maximum possible value of Ω turns out to be ~O(10^{-4}). Thus, one can neglect this effect while obtaining the temperature distribution. In this context, it also needs to be mentioned that the flow physics here is governed by non-isothermal electro-osmosis where no pressure gradient is externally imposed. Any kind of pressure gradient is induced only because of the imbalance between the pertinent electrokinetic forces, and, thus, the resulting electro-osmotic velocity is small enough to make the viscous dissipation effect insignificant. Using this, the simplified form of the energy equation takes the following form:

$$\rho C_p\left(u\frac{\partial T}{\partial x}+v\frac{\partial T}{\partial y}\right)=\frac{\partial}{\partial x}\left\{k_{\mathrm{eff}}\frac{\partial T}{\partial x}\right\}+\frac{\partial}{\partial y}\left\{k_{\mathrm{eff}}\frac{\partial T}{\partial y}\right\}+\sigma_{\mathrm{eff}}\left\{\left(\frac{\mathrm{d}\phi}{\mathrm{d}x}+\frac{\partial\psi}{\partial x}\right)^2+\left(\frac{\partial\psi}{\partial y}\right)^2\right\}. \tag{2.5}$$

Here, we introduce a new variable $\tilde{p}$ as $\tilde{p} = p - \varepsilon_{\mathrm{ref}}\kappa_0^2\psi^2/2$ [54,55] and rewrite the continuity and momentum equations in the following way:

$$\left.\begin{aligned} &\frac{\partial u}{\partial x}+\frac{\partial v}{\partial y}=0\\ &0=-\frac{\partial\tilde{p}}{\partial x}+\frac{\partial\tau_{xx}}{\partial x}+\frac{\partial\tau_{yx}}{\partial y}+F_{bx}+\varepsilon_{\mathrm{eff}}\kappa_0^2\psi\frac{\partial\psi}{\partial x}\\ &0=-\frac{\partial\tilde{p}}{\partial y}+\frac{\partial\tau_{xy}}{\partial x}+\frac{\partial\tau_{yy}}{\partial y}+F_{by}+\varepsilon_{\mathrm{eff}}\kappa_0^2\psi\frac{\partial\psi}{\partial y} \end{aligned}\right\}. \tag{2.6}$$

In this study, we consider the simplified Phan–Thien Tanner (sPTT) model [85] to simulate the viscoelastic fluid characteristics [37,39,40]. Therefore, in the above equation, the stress

Downloaded from https://royalsocietypublishing.org/ on 30 January 2023

components of the sPTT fluid take the form

$$\left.\begin{aligned} 2\mu_{\text{eff}}\frac{\partial u}{\partial x} &= F\,\tau_{xx} + \lambda_{\text{eff}}\left(u\frac{\partial \tau_{xx}}{\partial x} + v\frac{\partial \tau_{xx}}{\partial y} - 2\frac{\partial u}{\partial x}\tau_{xx} - 2\frac{\partial u}{\partial y}\tau_{yx}\right) \\ 2\mu_{\text{eff}}\frac{\partial v}{\partial y} &= F\,\tau_{yy} + \lambda_{\text{eff}}\left(u\frac{\partial \tau_{yy}}{\partial x} + v\frac{\partial \tau_{yy}}{\partial y} - 2\frac{\partial v}{\partial x}\tau_{xy} - 2\frac{\partial v}{\partial y}\tau_{yy}\right) \\ \mu_{\text{eff}}\left(\frac{\partial u}{\partial y} + \frac{\partial v}{\partial x}\right) &= F\,\tau_{xy} + \lambda_{\text{eff}}\left(u\frac{\partial \tau_{xy}}{\partial x} + v\frac{\partial \tau_{xy}}{\partial y} - \frac{\partial u}{\partial y}\tau_{yy} - \frac{\partial v}{\partial x}\tau_{xx}\right) \end{aligned}\right\}, \tag{2.7}$$

where F is the stress coefficient defined by $F = 1 + \delta\,\lambda_{\text{eff}}(\tau_{xx} + \tau_{yy})/\mu_{\text{eff}}$ with δ representing the extensibility of the viscoelastic fluid. In equation (2.7), μ_{eff} and λ_{eff} are the dynamic viscosity and relaxation time of the viscoelastic fluid which obey the following relationship: $\mu_{\text{eff}} = \mu_{\text{ref}}\exp[-\alpha_6(T - T_{\text{ref}})]$ and $\lambda_{\text{eff}} = \lambda_{\text{ref}}\exp[-\alpha_6(T - T_{\text{ref}})]$. Here, μ_{ref} and λ_{ref} are the reference values at T_{ref} with α_6 being the coefficient of temperature dependence [86]. For the physical boundary conditions, we employ the classical no-slip condition at the channel walls, while the ζ-potentials follow the axially modulated profiles depicted above. Isobaric and isothermal conditions are maintained at the two ends of the microchannel. The symmetry condition prevails at the channel centreline, while heat loss (q_w) occurs from the channel walls to the surrounding through natural convection, i.e. $q_w = h_T(T - T_{\text{ref}})$, where h_T is the convective heat transfer coefficient. Following this, the boundary conditions are represented in the following way:

$$\begin{aligned} &u(y = \pm h) = 0, \quad v(y = \pm h) = 0;\ p(x = 0) = p_{\text{atm}}, \quad p(x = l) = p_{\text{atm}}, \\ &T(x = 0) = T_{\text{ref}}, \quad T(x = l) = T_{\text{ref}};\ k_{\text{eff}}\left(\frac{\partial T}{\partial y}\right)\Big|_{y=\pm h} = \mp h_T\,(T - T_{\text{ref}}),\ \left(\frac{\partial T}{\partial y}\right)_{y=0} = 0, \\ &\phi(x = 0) = E_{\text{ref}}\,l = \phi_{\text{ref}}, \quad \phi(x = l) = 0; \quad \psi(y = \pm h) = \zeta = \zeta_{\text{ref}}\{\alpha_1 + \alpha_2\cos(\omega_t\,x)\}. \end{aligned} \tag{2.8}$$

For solving the velocity, temperature and potential distribution, we non-dimensionalize the equation using the following dimensionless variables:

$$\left.\begin{aligned} \bar{x} = \frac{x}{l},\ \bar{y} = \frac{y}{h},\ \bar{u} = \frac{u}{u_{\text{HS}}},\ \bar{v} = \frac{v\,l}{(u_{\text{HS}}\,h)},\ \bar{p} = \frac{(p - p_{\text{atm}})\,h^2}{(\mu_{\text{ref}}\,u_{\text{HS}}\,l)},\ \bar{T} = \frac{T - T_{\text{ref}}}{\Delta\,T} \\ \bar{\tau}_{xx} = \frac{\tau_{xx}\,h}{\mu_{\text{eff}}\,u_{\text{HS}}},\ \bar{\tau}_{yy} = \frac{\tau_{yy}\,h}{\mu_{\text{eff}}\,u_{\text{HS}}},\ \bar{\tau}_{yx} = \frac{\tau_{yx}\,h}{\mu_{\text{eff}}\,u_{\text{HS}}},\ \bar{\phi} = \phi/\phi_{\text{ref}},\ \bar{\psi} = \frac{\psi}{\zeta_{\text{ref}}} \end{aligned}\right\}, \tag{2.9}$$

where $u_{\text{HS}} = -\varepsilon_{\text{ref}}\,\zeta_{\text{ref}}\,E_{\text{ref}}/\mu_{\text{ref}}$ is the Helmholtz–Smoluchowski velocity, the characteristic velocity scale for the EOF and ΔT is the characteristic temperature difference defined as $\Delta\,T \sim \sigma_{\text{ref}}{E_{\text{ref}}}^2\,h\,l/k_{\text{ref}}$ obtained by equating the conduction term to the heat generation term in the energy equation. The dimensionless forms of the governing equations along with the solution procedure are discussed in detail in electronic supplementary material, section A.

(a) Dispersion coefficient

We have considered the dispersion occurring owing to an interaction between the electric field and flow field combined with the charge modulated surface. From definition, the dispersion coefficient (D_{eff}) is related to the solute distribution in the following way [25]:

$$D_{\text{eff}} = \frac{1}{2}\frac{\mathrm{d}}{\mathrm{d}t}\sigma^2(t), \tag{2.10}$$

where σ^2 is the variance in the solute displacement band which, in turn, is related to the plate height ($\tilde{h}$) as

$$\tilde{h} = \frac{\mathrm{d}}{\mathrm{d}\tilde{x}}\sigma^2(\tilde{x}), \tag{2.11}$$

Downloaded from https://royalsocietypublishing.org/ on 30 January 2023

with $\tilde{x}$ being the centre of mass of the band. Thus, σ^2 and $\tilde{x}$ are the two parameters which are associated with the band broadening phenomenon where the velocity of the centre of mass is

$$\tilde{u} = \frac{\mathrm{d}\tilde{x}}{\mathrm{d}t}, \tag{2.12}$$

Now, combining these two equations, one can rewrite the dispersion coefficient (D_{eff}) as follows:

$$D_{\mathrm{eff}} = \frac{\tilde{u}\,\tilde{h}}{2}, \tag{2.13}$$

where $\tilde{u}$ also represents the cross-sectional averaged flow velocity through the microchannel and the plate height $\tilde{h}$ is evaluated by

$$\tilde{h} = \frac{2D}{\tilde{u}} + \left(\frac{\tilde{u}\,h^{*2}}{8D}\right), \tag{2.14}$$

where D is the molecular diffusivity coefficient and h^* is the minimum plate height which is given by the following equation [25]:

$$h^* = 16\int_0^h \int_0^y \left[\left\{\left(\frac{u}{\tilde{u}}\right) - 1\right\}\mathrm{d}y\right]^2 \frac{\mathrm{d}y}{h}. \tag{2.15}$$

Now, the dimensionless form of equation (2.13) becomes

$$\bar{D}_{\mathrm{eff}} = 1 + \frac{\left(\mathrm{Pe_D}\,\bar{\tilde{u}}\,h^*\right)^2}{16}, \tag{2.16}$$

where $\bar{D}_{\mathrm{eff}}$ is the dimensionless dispersion coefficient, $\mathrm{Pe_D}$ is the Peclet number for dispersion and $\bar{\tilde{u}}$ is the dimensionless average velocity. As clear from the definition of $\bar{D}_{\mathrm{eff}}$, it depends strongly on the flow field. This flow field, in turn, is a function of the acting electrokinetic forces which are modulated by the induced temperature gradient, thus establishing a strong dependence of $\bar{D}_{\mathrm{eff}}$ with temperature.

3. Results and discussions

While we have performed simulations over a wide range of physically plausible problem data, we have collapsed the results in terms of the pertinent non-dimensional numbers. Towards that, the corresponding estimates of various dimensional parameters have been taken as $h \sim 10 - 10^2$ μm, $l \sim 1 - 10$ mm, $\rho \sim 10^3\,\mathrm{kg\,m^{-3}}$, $C_p = 4200\,\mathrm{J\,kg^{-1}\cdot K}$, $E_{\mathrm{ref}} \sim 10^3 - 10^4\,\mathrm{V\,m^{-1}}$, $\zeta_{\mathrm{ref}} \sim 10^{-2}$V, $\mu_{\mathrm{ref}} \sim 10^{-3}$Pa s, $\sigma_{\mathrm{ref}} \sim 10^{-2} - 10^{-1}\,\mathrm{S\,m^{-1}}$, $k_{\mathrm{ref}} \sim 0.613\,\mathrm{W/(mK)}$, $\varepsilon_{\mathrm{ref}} \sim 10^{-10}\,\mathrm{CV^{-1}}m^{-1}$, $\lambda_{\mathrm{ref}} \sim 10^{-3} - 10^{-1}$ s, $T_{\mathrm{ref}} \sim 298\,K, D \sim 10^{-9}\,\mathrm{m^2 s^{-1}}$, $\Delta T \sim 1 - 10^2$ K, $\lambda_D \sim 1 - 100$ nm, $\alpha_3 \sim 10^{-3}\ \mathrm{K^{-1}}$, $\alpha_4 \sim 10^{-2}\ \mathrm{K^{-1}}$, $\alpha_5 \sim 10^{-3}\ \mathrm{K^{-1}}$ and $\alpha_6 \sim 10^{-2}\ \mathrm{K^{-1}}$.

Before presenting the results, we first show here how our present analysis emulates previous experimental outcomes. We have compared our theoretical predictions of average velocity for non-isothermal EOF with that of Venditti *et al*. [87]. As depicted in figure 1 of their work, EOF velocity in PDMS-based microchannel using 10 mM KCl solution showed a linear dependence with temperature from 313 to 333 K and beyond 333 K, nonlinear behaviour is observed attributed to the highly pronounced Joule heating effect. In our present analysis, while demonstrating the effect of thermal perturbation on the flow field, we have used ξ as a perturbation parameter where the results are presented up to $\xi = 0.3$. From the definition of ξ, it is clear that ξ depends on two factors, one is the temperature sensitivity parameter α_6 (responsible for making viscosity and relaxation time of fluid to be temperature-dependent) while another one being the temperature difference (ΔT) induced within the flow domain. The maximum temperature difference (ΔT) up to which linear thermal effect prevails is 20 K. This ΔT along with $\xi = 0.3$ results in the value of the temperature sensitivity coefficient (α_6) to be $\sim 0.015\,\mathrm{K^{-1}}$, typically observed in the physical property variations in non-isothermal flows [88,89].

While comparing with Venditti *et al*. [87], we have presented our results of non-isothermal EOF velocities at $\alpha_1 = 1$, $\alpha_2 = 0$, $\mathrm{De} = 0$, $\chi = 0.01$, $\mathrm{Pe_T} = 0.01$, $\mathrm{Pe_D} = 5$, $\nu = 0.006$ and $\alpha_4 = 0.01$.

Downloaded from https://royalsocietypublishing.org/ on 30 January 2023

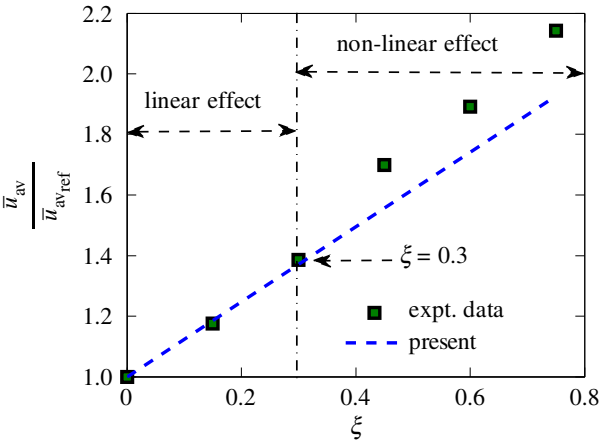

Figure 2. Comparison between the present theoretical predictions with that of Venditti *et al*. [87]. Symbols represent the experimental outcomes, whereas the dotted line corresponds to the present asymptotic solution. (Online version in colour.)

Using typical values of the parameters like $h \sim O(10)\,\mu$m, $l \sim O(1)$ mm, $E_{ref} \sim O(10^4)$Vm^{-1}, $\rho \sim O(10^3)$ kg m^{-3}, $C_p \sim O(10^3)$ J kg^{-1} K^{-1}, $\Delta T \sim$ O(10)K, $u_{HS} \sim$ O(10^{-3})m s^{-1}, $\mu_{ref} \sim O(10^{-3})$ Pa s, $\sigma_{ref} \sim$ O(10^{-1}) S m^{-1}, $k_{ref} \sim O(1)$W m^{-1} K^{-1}, $D \sim O(10^{-9})$ m^2 s^{-1} and $h_T \sim O(10^2)$W m^{-2} K^{-1}, the values of the dimensionless quantities are $\chi \sim$ O(10^{-2}), Pe$_T \sim$ O(10^{-2}), Pe$_D \sim$ O(10) and $\nu \sim$ O(10^{-3}), respectively, which are in accordance with the values used for comparison. Also, $\alpha_1 = 1$ and $\alpha_2 = 0$ represent the EOF with uniform zeta potential (i.e. the axially varying component remains absent), while De $= 0$ corresponds to Newtonian fluid. As evident from figure 2, our asymptotic solution closely matches with the experimental data up to $\xi = 0.3$ and as we start increasing ξ beyond 0.3, deviation with experimental results comes into prominence with ~10% underestimation in asymptotic solution being observed at $\xi = 0.75$. As our asymptotic solution is only able to capture linear variation with temperature, one needs to employ a numerical solution to incorporate this nonlinear thermal effect beyond $\xi = 0.3$. Considering this limitation in the present analysis, we have presented our results up to $\xi = 0.3$.

The axial variation of the dimensionless electrothermal force (i.e. the force that originates due to variations in electrical properties with temperature) is shown in figure 3*a*. Under isothermal condition ($\xi = 0$), the electric field remains unaffected along the microchannel. As we increase the value of ξ, the temperature field is induced which strongly influences the electrothermal force in the axial direction. As the electric field in the non-isothermal condition depends on the temperature distribution, it gets distorted with increasing ξ. When the channel surface is maintained at constant zeta potential (i.e. $\alpha_2 = 0$), the electrothermal force ($\bar{F}_x$) remains constant for the isothermal condition, i.e. $\xi = 0$. In a non-isothermal scenario, $\bar{F}_x$ starts to deviate from its constant value and gets amplified in the region where steep temperature gradients occur. The interaction between the temperature gradient and the surface potential gives rise to an enhancement of the electrothermal force up to two times at the channel ends (at $\xi = 0.3$), as clearly seen from figure 3*a*. In the absence of any thermal perturbation, the axially modulated potentials result in a harmonic distribution of the electrokinetic force, with the minima shifted from $\bar{x} = 0.65$ to $\bar{x} = 0.5$. Nevertheless, as we increase the value of ξ, non-trivial interaction between the modulated wall potential and the Joule heating effect affects the imposed temperature gradients at both ends, thereby resulting in an irregular distribution of $\bar{F}_x$.

The pressure distribution along the x-direction is demonstrated in figure 3*b*. For constant zeta potential, the pressure distribution remains identical for a Newtonian fluid and its viscoelastic counterparts. With increasing ξ, the interaction between the thermal gradients and the electrokinetic force leads to an imbalance in the pressure distribution, creating over pressure

Downloaded from https://royalsocietypublishing.org/ on 30 January 2023

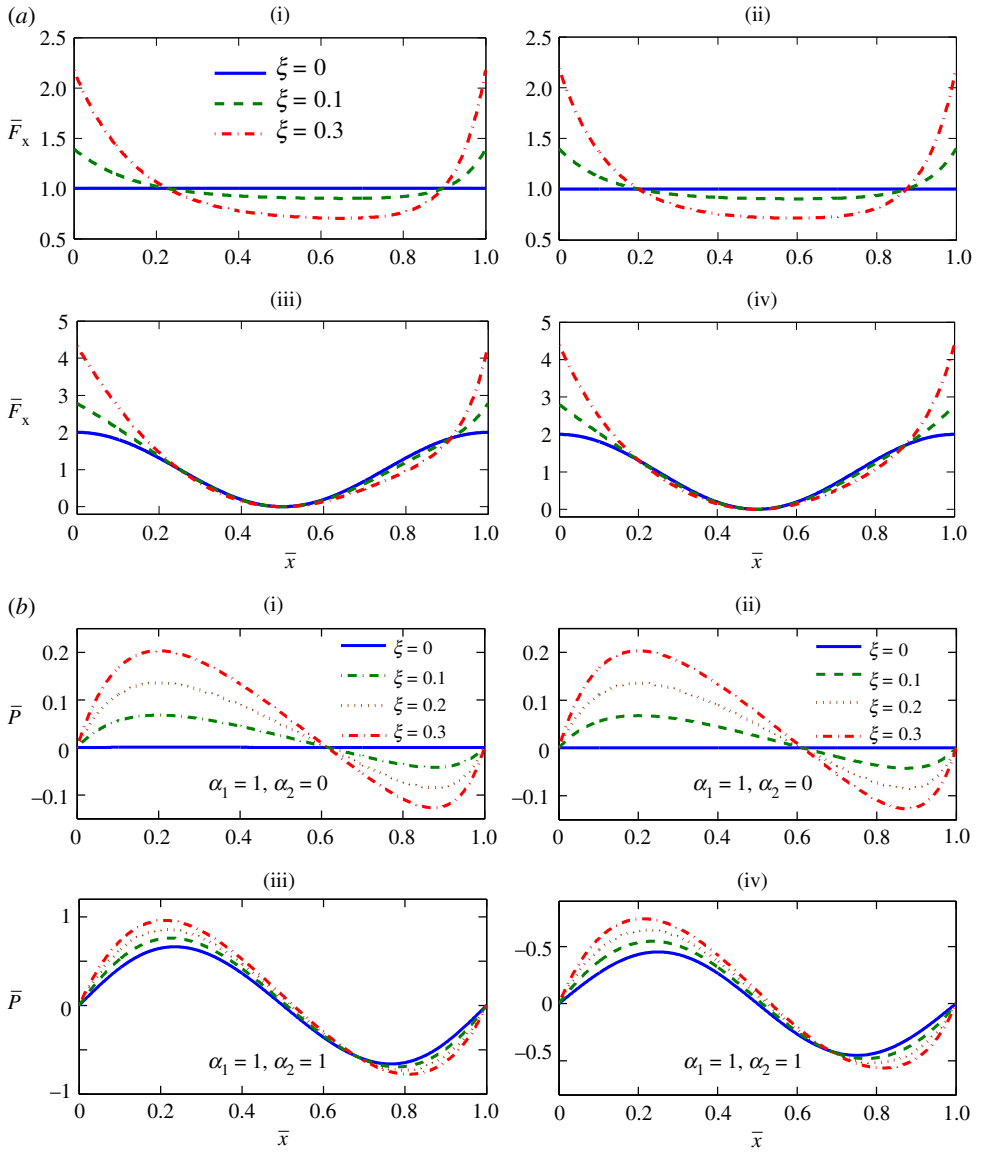

Figure 3. (*a*) The axial variation of the electrothermal force for different values of ξ. (i,iii) Viscoelastic fluid De = 0.5. (ii,iv) Newtonian fluid De = 0. Also, (i,ii) represent constant zeta potential $\alpha_2 = 0$, while (iii,iv) represent axially modulated zeta potential $\alpha_2 = 1$. (*b*) Distribution of pressure in the *x*-direction for different α_2. For (i,ii), $\alpha_2 = 0$; for (iii,iv), $\alpha_2 = 1$. Also (i,iii) account for viscoelastic fluids, while (ii,iv) show its Newtonian counterpart. (Online version in colour.)

towards the inlet and low pressure at the outlets which, in turn, affects the electrothermal force. Irrespective of the value of ξ, the interacting forces balance each other at $\bar{x} \sim 0.6$ (thus $\bar{x} \sim 0.6$ becomes the region of the onset of imbalance between the counteracting forces), thus resulting in zero-induced pressure. By contrast, the interaction between the thermal gradients and the modulated zeta potential strongly influences the pressure distribution which is further strengthened in viscoelastic fluids, as can be seen from figure 3*b*.

The increment in the volumetric flow rate is manifested in figure 4*a*, where $\bar{Q}$ is plotted as a function of the patterning frequency. The net throughput basically depends on the interaction between the modulated electrokinetic forces and the temperature gradients. This interaction

Downloaded from https://royalsocietypublishing.org/ on 30 January 2023

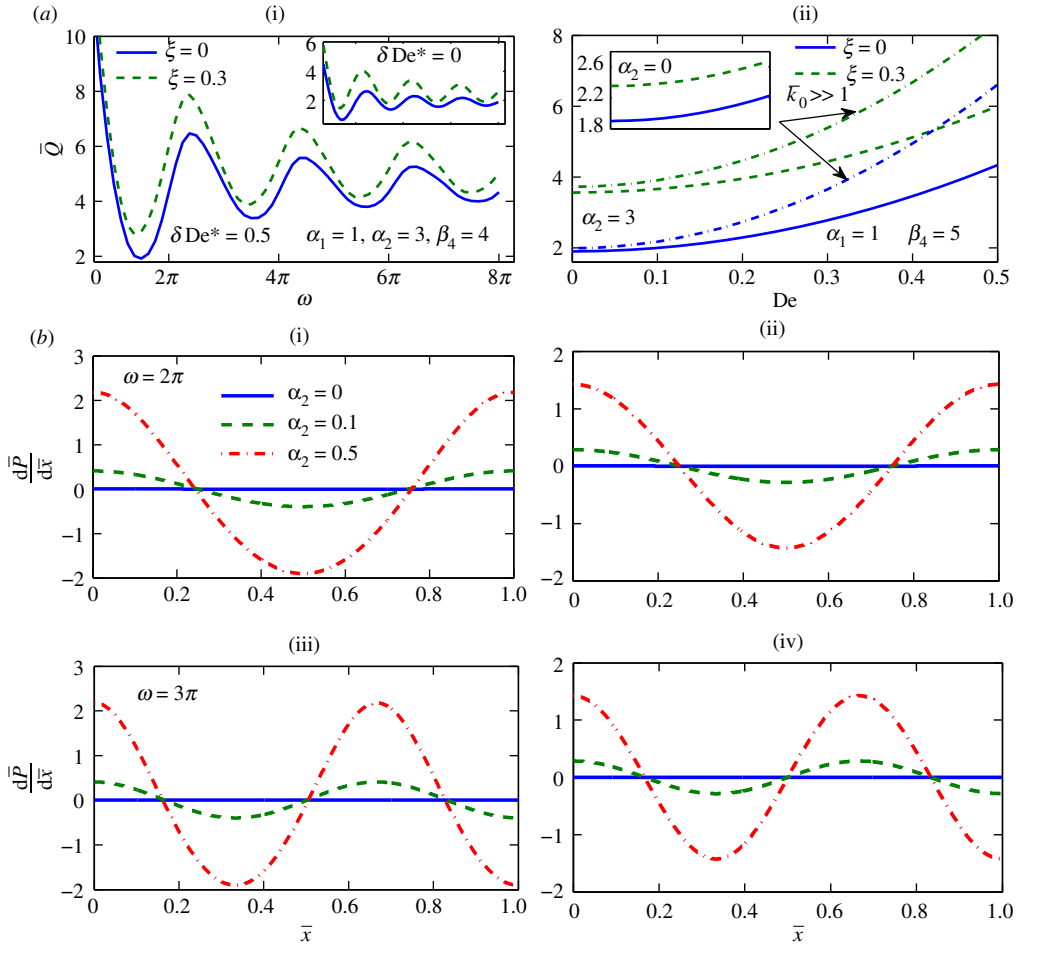

Figure 4. (*a*) (i) The variation of the volumetric flow rate as a function of patterning frequency for De = 0.5. (Inset corresponds to the Newtonian fluid.) (ii) Dependence of $\bar{Q}$ on Deborah number (De) evaluated at $\alpha_2 = 3$ (inset for $\alpha_2 = 0$). The predictions in the thin EDL limit are shown by dash-dot lines. (*b*) The axial variation of the pressure gradient for different patterning frequencies. (i,ii) correspond to $\omega = 2\pi$, while (iii,iv) are for $\omega = 3\pi$. Also, (i,iii) account for viscoelastic fluids, while (ii,iv) show its Newtonian counterpart. (Online version in colour.)

makes the distribution of the flow rate periodic in nature where the degree of periodicity depends on the direction of the electrothermal force and the temperature gradients, dictated by the patterning frequency of modulation. Figure 4*a* also includes the variation of $\bar{Q}$ with the increasing Deborah number (De). Increasing the value of De is associated with the pronounced shear-thinning behaviour which leads to significant augmentation in the flow rate. It increases linearly up to a certain value of Deborah number, De ~ 0.05. Then, it changes its linearity and increases abruptly following an exponential behaviour. Now, the imposed non-isothermal condition induces electrothermal interaction and results in the reduction of the viscosity of the fluid thus leading to the increment of the flow rate as a consequence. In case of a thin EDL limit, the nonlinear behaviour is observed earlier (i.e. at low values of De).

The distribution of the pressure gradient is illustrated in figure 4*b*. No pressure gradient is induced in the x-direction when the channel walls are subjected to uniform wall potential and the corresponding velocity profile is plug flow type, typically observed in purely EOFs. Conversely, increasing the value of α_2 strongly influences the hydrodynamics of the flow by creating adverse pressure gradient at both ends and favourable pressure gradient in the middle. In the presence of

Downloaded from https://royalsocietypublishing.org/ on 30 January 2023

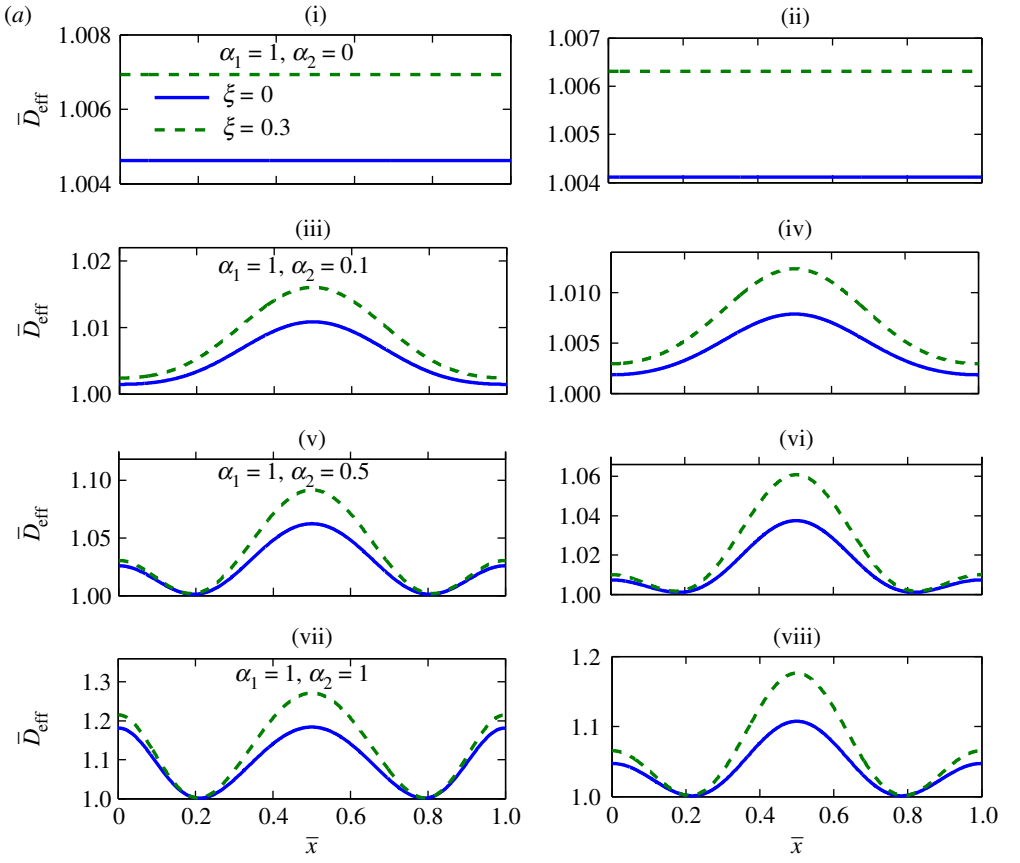

Figure 5. (*a*) The dependence of the dispersion coefficient in the *x*-direction for different values of α_2. In (i,ii), $\alpha_2 = 0$, (iii,iv) $\alpha_2 = 0.1$, (v,vi) $\alpha_2 = 0.5$, (vii,viii) $\alpha_2 = 1$. Also, (i,iii,v) account for viscoelastic fluid De = 0.5, (ii,iv,vi) for Newtonian fluid. (*b*) The effect of patterning frequency on the axial variation of the dispersion coefficient. Results are shown for two different values of ξ. (i,iii,v,vii) viscoelastic fluid (De = 0.5) and (ii,iv,vi,viii) Newtonian fluid (De = 0). (*c*) The parametric variation (α_1 and α_2) of the dispersion coefficient in the presence of thermal perturbation. (i,iii,v) Viscoelastic fluid (De = 0.5) and (ii,iv,vi) Newtonian fluid (De = 0). (*d*) The enhancement in the dispersion coefficient for different values of β_4. Inset (i) shows the effect of both Pe_0 and $\bar{\kappa}_0$ with increasing β_4, while (ii) corresponds to decreasing β_4 (evaluated at $\omega = 2\pi$). (Online version in colour.)

adverse pressure gradient, the flow field is distorted which becomes more pronounced at higher values of α_2. But, favourable pressure gradient results in a convex type of velocity profile and the degree of convexity increases with higher potential modulation (α_2). For the patterning frequency $\omega = 2\pi$, the modulated electrokinetic force at the two ends is in the same direction (both positive) while changing the patterning frequency from $\omega = 2\pi$ to $\omega = 3\pi$ makes the forces opposite in the two ends (positive at the inlet and negative at the exit). Also, the region of favourable pressure gradient occurs much earlier due to the imbalance between the forces, as evident from figure 4*b* where the minima is shifted to $\bar{x} = 0.35$ from $\bar{x} = 0.5$ (for the previous case) and the maxima occurs at $\bar{x} = 0.67$, much earlier than the channel exit (which is the location of maxima for $\omega = 2\pi$).

In this context, it needs to be mentioned that the results are reported herein for De up to ~0.5. For small values of De, the pressure distribution for viscoelastic fluid and its Newtonian counterpart shows similar behaviour [86]. However, increasing De beyond 0.5 would lead to more pressure induction due to a highly pronounced shear-thinning effect. Also, we have chosen the linear sPTT model to describe the rheological behaviour of a viscoelastic fluid, which is essentially

Downloaded from https://royalsocietypublishing.org/ on 30 January 2023

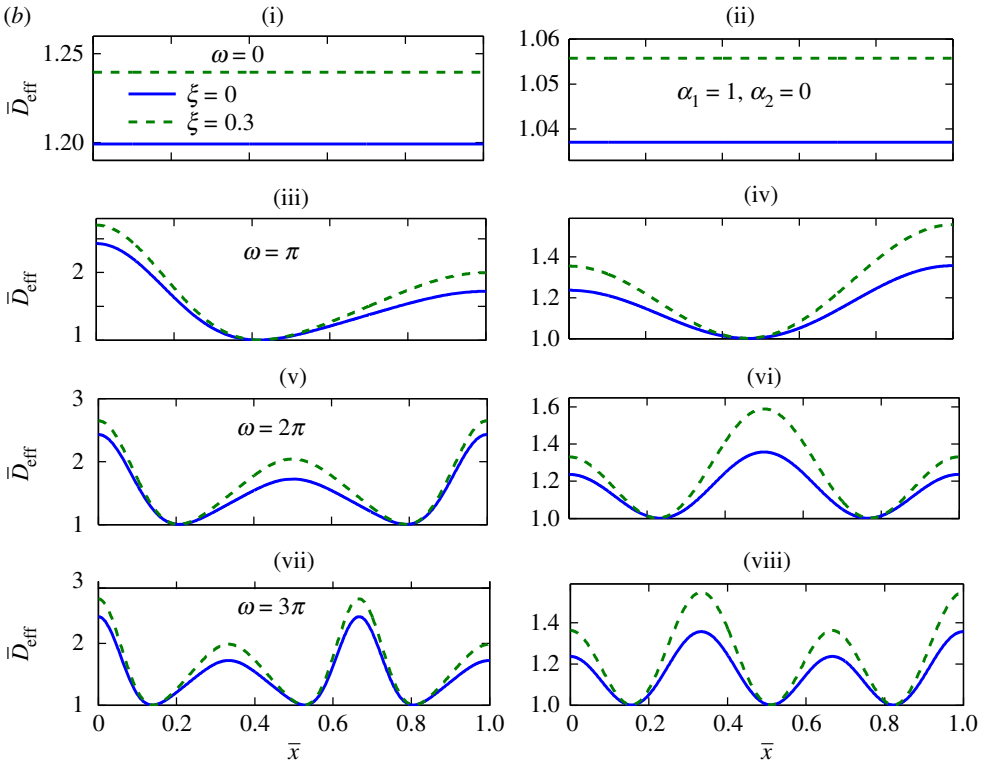

Figure 5. (*Continued.*)

an approximation of the exponential sPTT model. This approximation holds well only for small values of De [40] and hence, the upper limit of De has been chosen accordingly.

The axial variation of the solute dispersion coefficient is depicted in figure 5*a* where the effect of the varying zeta potential is shown for a fixed patterning frequency ($\omega = 2\pi$). In the absence of any modulation in zeta potential (i.e. $\alpha_2 = 0$), the corresponding dispersion coefficient is very close to unity which is enhanced slightly in the case of a viscoelastic fluid (De = 0.5). As we start increasing the value of α_2, the modulated zeta potential alters the velocity distribution significantly and it no longer remains uniform in the axial direction, which influences strongly the distribution of the dispersion coefficient along the channel. As adverse pressure gradient prevails up to $\bar{x} = 0.2$, the velocity profile is distorted and follows a concave shape which results in the reduction of the dispersion coefficient and the reduction becomes more prominent at higher modulation (α_2) of surface potential (for $\alpha_2 \geq 0.5$). Increasing α_2 induces more non-uniformity in the flow field, thereby influencing the velocity gradient strongly. Similarly, a favourable pressure gradient is prevalent at the middle of the channel which results in an extra contribution in dispersion in addition to the purely diffusional dispersion. As a result, the dispersion coefficient is enhanced significantly with the maximum increment of ~10.5 % observed at $\bar{x} = 0.5$.

Besides, the effect of viscoelasticity on the dispersion coefficient is also reflected in figure 5*a*. Increasing De augments the shear-thinning behaviour of the fluid resulting in an enhancement of $\bar{D}_{\text{eff}}$ up to ~18 %, as clear from figure 5*a*(v). It is important to mention that the effect of viscoelasticity is notable only in the favourable pressure gradient region and less significant in the adverse pressure gradient region. Now, the introduction of the non-isothermal condition induces an electrothermal force which affects the flow field strongly. The presence of temperature gradients at both ends makes the electrothermal force maximum at those locations, while at the middle, it becomes minimum. Accordingly, the maximum enhancement of $\bar{D}_{\text{eff}}$ is observed at $\bar{x} = 0.5$. Also, increasing the degree of non-uniformity in zeta potential results in the reduction

Downloaded from https://royalsocietypublishing.org/ on 30 January 2023

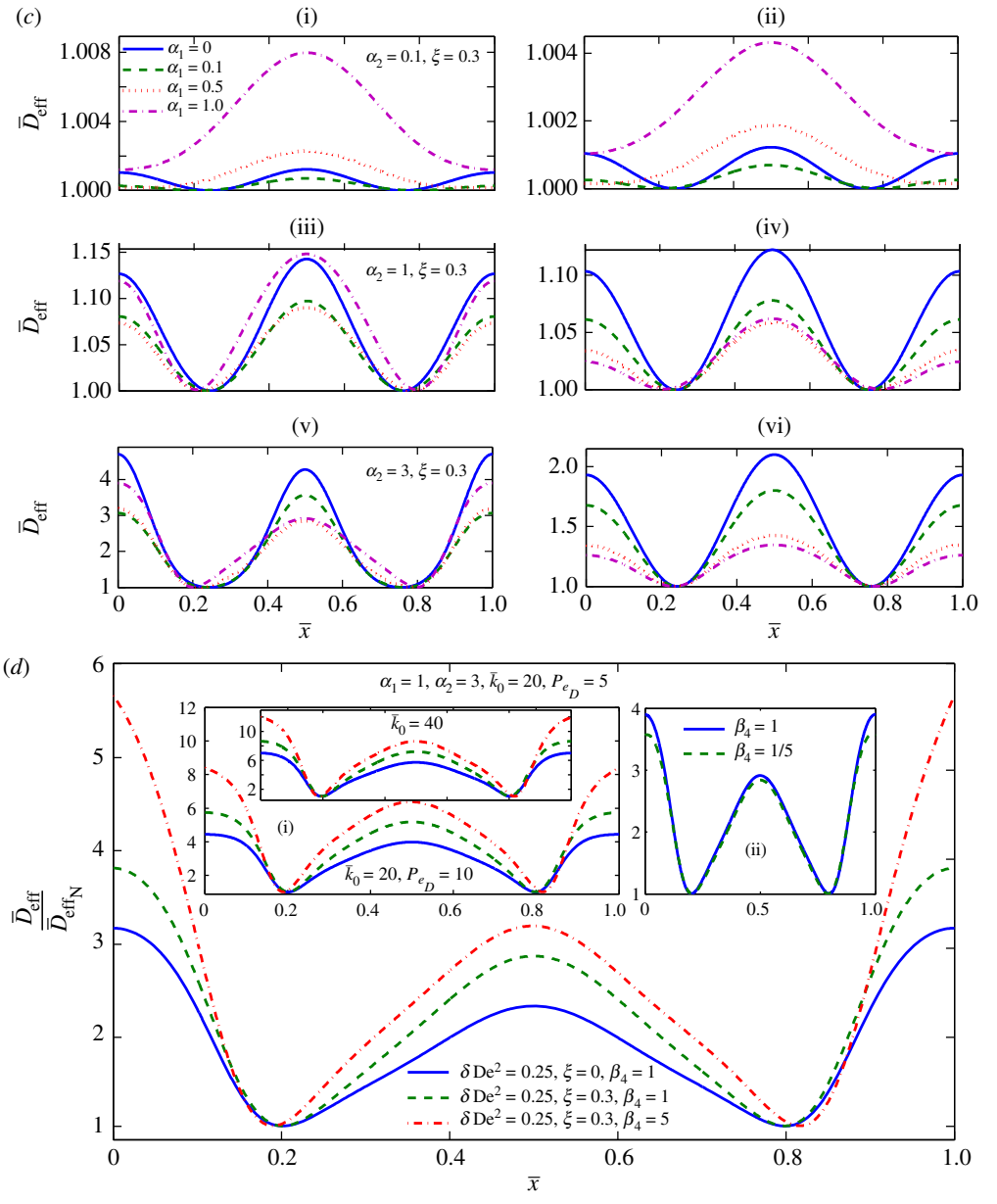

Figure 5. (*Continued.*)

of the electrothermal force and $\bar{D}_{\text{eff}}$ is increased up to ~25% by changing the value of α_2 from 0.1 to 1.

The effect of patterning frequency on the dispersion coefficient is highlighted in figure 5*b*. $\omega = 0$ means that the axially varying component of the electrokinetic force is absent and the dispersion coefficient remains constant which is further enhanced on imposition of a non-isothermal condition ($\xi = 0.3$). One interesting thing to observe here is that the distribution of $\bar{D}_{\text{eff}}$ is altered drastically as we change the patterning frequency from $\omega = \pi$ to $\omega = 2\pi$ and $\omega = 2\pi$ to $\omega = 3\pi$. Contrary to $\omega = 2\pi$, the electrokinetic force is modulated in the opposite way for $\omega = \pi$ and $\omega = 3\pi$. For $\omega = \pi$, adverse pressure gradient is induced up to the channel centreline, thus diminishing the extent of dispersion. Increasing ω induces both pressure gradients with

Downloaded from https://royalsocietypublishing.org/ on 30 January 2023

the region of occurrence depending on the patterning frequency. As a result, two regions of favourable pressure gradients are induced (shown earlier in figure 4*b*) and two peaks are observed in $\omega = 3\pi$ instead of one ($\omega = 2\pi$) in the distribution of the dispersion coefficient. For the sake of brevity, the corresponding results in the thin EDL limit are presented and discussed in electronic supplementary material, section G.

We now proceed to depict in figure 5*c* the relative contribution of the potential modulation parameters in the presence of thermal perturbation (i.e. α_1 and α_2), where α_1 and α_2 are the axially invariant and variant components. For lower values of α_2 (i.e. $\alpha_2 = 0.1$), increasing α_1 results in Gaussian-type distribution of the dispersion coefficient. When these two components are comparable to each other, it results in a reduction of $\bar{D}_{\text{eff}}$ (figure 5*c* (i,ii)). As the invariant component becomes dominant, it plays a decisive role in determining the mode of dispersion, as observed in figure 5*c* (i,ii). It is interesting to note that, at $\alpha_2 = 1$, most of the trends are similar except for higher α_1 where the effect of fluid viscoelasticity prevails over the invariant component, as observed in figure 5*c*(iii). Finally, for higher α_2, the effect of axial modulation becomes so dominant over the invariant one that even fluid viscoelasticity remains overshadowed (shown in figure 5*c*(v)).

The enhancement in the dispersion coefficient along the axial direction is illustrated in figure 5*d* where $\bar{D}_{\text{eff}}$ is the effective dispersion coefficient, while $\bar{D}_{\text{eff}_N}$ corresponds to that of the Newtonian fluid in the absence of any thermal perturbation. Introducing thermal perturbation gives rise to concomitant augmentation in the dispersion coefficient which is further amplified near the two ends of the microchannel as we increase the value of β_4. $\beta_4 = \alpha_4/\alpha_6$ is essentially the ratio of the temperature coefficients of the electrical conductivity and dynamic viscosities of the fluid, i.e. their relative temperature sensitivity. Increasing the value of β_4 implicates that the electrical conductivity is more susceptible to any change in temperature when compared with viscosity. This results in significant enhancement in the modulated electrokinetic forces thus creating more favourable pressure gradient with massive increment at the channel ends, which is clearly reflected at the respective dispersion coefficients. For the patterning frequency $\omega = 2\pi$, the electrokinetic forces act in the same direction and when this is coupled with the temperature sensitivity parameter, one can observe a massive augmentation in the dispersion coefficient up to approximately six times, as can be seen from figure 5*d*. Conversely, if we decrease the value of β_4, the reduction in viscosity with temperature becomes more prominent which results in lowering the pressure gradient thereby yielding reduced dispersion coefficient (shown in the inset (ii) of figure 5*d*), although the effect is inappreciable (the ratio becomes $\sim$3.6 from $\sim$4). Figure 5*d* also shows the prediction of the dispersion coefficient at higher values of Pe_D; the higher the value of Pe_D means a larger diffusional dispersion. Such a dispersion is in conjunction with the additional effects rising from the interaction between thermal and electrokinetic forces, thus giving rise to further augmentation up to $\sim$8 times with respect to the Newtonian fluid. Additionally, if we increase the value of $\bar{\kappa}_0$, the region of excess charge distribution becomes less and the respective dispersion coefficient is further enhanced up to $\sim$12 times as can be clearly seen from the inset of figure 5*d*.

4. Conclusion

In this study, we have brought out a unique coupling between modulated surface charges and local temperature gradients towards realizing giant augmentations in dispersion coefficients for electro-osmotic flow of viscoelastic fluids. As the classical EOF results in a uniform velocity profile, it attenuates the dispersion and mixing. In this context, the present study reveals that, by exploiting an intricate interplay between the fluid rheology and the coupled modulation of electrical and thermal fields, one may achieve massive augmentation in the hydrodynamic dispersion without compromising the volumetric flow rate. Such significantly augmented dispersion characteristics may be of utilitarian importance in improved design of microfluidic devices demanding augmented dispersion and mixing performance without sacrificing the net throughput.

Downloaded from https://royalsocietypublishing.org/ on 30 January 2023

Data accessibility. The asymptotic analysis and the consequent analytical expressions given in the electronic supplementary material which consists of a pdf file.

Authors' contributions. S.C. conceptualized the work. S.M. and J.D. performed the analysis. All four authors contributed equally in drafting the manuscript.

Competing interests. The authors have no competing interests.

Funding. The authors gratefully acknowledge the financial support provided by the Indian Institute of Technology Kharagpur (sanction letter no.: IIT/SRIC/ATDC/CEM/2013-14/118, dated 19.12.2013).

References

1. Whitesides GM. 2006 The origins and the future of microfluidics. *Nature* **442**, 368–373. (doi:10.1038/nature05058)
2. Stone HA, Stroock AD, Ajdari A. 2004 Engineering flows in small devices. *Annu. Rev. Fluid Mech.* **36**, 381–411. (doi:10.1146/annurev.fluid.36.050802.122124)
3. Stroock AD, Dertinger SKW, Ajdari A, Mezic I, Stone HA, Whitesides GM. 2002 Chaotic mixer for microchannels. *Science* **295**, 647–651. (doi:10.1126/science.1066238)
4. Chang C-CC, Yang R-JJ. 2008 Chaotic mixing in a microchannel utilizing periodically switching electro-osmotic recirculating rolls. *Phys. Rev. E* **77**, 1–10. (doi:10.1103/PhysRevE.77.056311)
5. Sugioka H. 2010 Chaotic mixer using electro-osmosis at finite Péclet number. *Phys. Rev. E Stat. Nonlinear, Soft Matter Phys.* **81**, 1–9. (doi:10.1103/PhysRevE.81.036306)
6. Zhang J, He G, Liu F. 2006 Electro-osmotic flow and mixing in heterogeneous microchannels. *Phys. Rev. E* **73**, 56305. (doi:10.1103/PhysRevE.73.056305)
7. Glasgow I, Batton J, Aubry N. 2004 Electroosmotic mixing in microchannels. *Lab. Chip* **4**, 558–562. (doi:10.1039/B408875A)
8. Anderson PD, Galaktionov OS, Peters GWM, van de Vosse FN, Meijer HEH. 2000 Mixing of non-Newtonian fluids in time-periodic cavity flows. *J. Nonnewton. Fluid Mech.* **93**, 265–286. (doi:10.1016/S0377-0257(00)00120–8)
9. Hunter RJ. 1981 *Zeta potential in colloid science*. London: Academic Press.
10. Probstein RF. 1994 *Physicochemical hydrodynamics: an introduction*, 2nd edn. New York: Wiley.
11. Karniadakis G, Beskok A, Aluru N. 2005 *Microflows and nanoflows*. Berlin, Germany: Springer.
12. Taylor G. 1953 Dispersion of soluble matter in solvent flowing slowly through a tube. *Proc. R. Soc. A* **219**, 186–203. (doi:10.1098/rspa.1953.0139)
13. Taylor G. 1954 Conditions under which dispersion of a solute in a stream of solvent can be used to measure molecular diffusion. *Proc. R. Soc. A* **225**, 473–477. (doi:10.1098/rspa.1954.0216)
14. Aris R. 1956 On the dispersion of a solute in a fluid flowing through a tube. *Proc. R. Soc. A* **235**, 67–77. (doi:10.1098/rspa.1956.0065)
15. Aris R. 1959 On the dispersion of a solute by diffusion, convection, and exchange between phases. *Proc. R. Soc. A* **252**, 538–550. (doi:10.1098/rspa.1959.0171)
16. Aris R. 1960 On the dispersion of a solute in pulsating flow through a tube. *Proc. R. Soc. A Math. Phys. Eng. Sci.* **259**, 370–376. (doi:10.1098/rspa.1960.0231)
17. Rana J, Murthy PVSN. 2016 Unsteady solute dispersion in non-Newtonian fluid flow in a tube with wall absorption. *Proc. R. Soc. A* **472**, 20160294. (doi:10.1098/rspa.2016.0294)
18. Rana J, Murthy PVSN. 2017 Unsteady solute dispersion in small blood vessels using a two-phase Casson model. *Proc. R. Soc. A* **473**, 20170427. (doi:10.1098/rspa.2017.0427)
19. Zholkovskij EK, Masliyah JH, Czarnecki J. 2003 Electroosmotic dispersion in microchannels with a thin double layer. *Anal. Chem.* **75**, 901–909. (doi:10.1021/ac0203591)
20. Zholkovskij EK, Masliyah JH. 2004 Hydrodynamic dispersion due to combined pressure-driven and electroosmotic flow through microchannels with a thin double layer. *Anal. Chem.* **76**, 2708–2718. (doi:10.1021/ac0303160)
21. Ajdari A, Bontoux N, Stone HA. 2006 Hydrodynamic dispersion in shallow microchannels: the effect of cross-sectional shape. *Anal. Chem.* **78**, 387–392. (doi:10.1021/ac0508651)
22. Dutta D. 2008 Electrokinetic transport of charged samples through rectangular channels with small zeta potentials. *Anal. Chem.* **80**, 4723–4730. (doi:10.1021/ac7024927)
23. Jansons KM. 2006 On Taylor dispersion in oscillatory channel flows. *Proc. R. Soc. A* **462**, 3501–3509. (doi:10.1098/rspa.2006.1745)

Downloaded from https://royalsocietypublishing.org/ on 30 January 2023

24. Ghosal S. 2002 Lubrication theory for electro-osmotic flow in a microfluidic channel of slowly varying cross-section and wall charge. *J. Fluid Mech.* **459**, 103–128. (doi:10.1017/S0022112002007899)
25. Arcos JC, Méndez F, Bautista EG, Bautista O. 2018 Dispersion coefficient in an electro-osmotic flow of a viscoelastic fluid through a microchannel with a slowly varying wall zeta potential. *J. Fluid Mech.* **839**, 348–386. (doi:10.1017/jfm.2018.11)
26. Berli CLA, Olivares ML. 2008 Electrokinetic flow of non-Newtonian fluids in microchannels. *J. Colloid Interface Sci.* **320**, 582–589. (doi:10.1016/j.jcis.2007.12.032)
27. Berli CLA. 2010 Electrokinetic energy conversion in microchannels using polymer solutions. *J. Colloid Interface Sci.* **349**, 446–448. (doi:10.1016/j.jcis.2010.05.083)
28. Das S, Chakraborty S. 2006 Analytical solutions for velocity, temperature and concentration distribution in electroosmotic microchannel flows of a non-Newtonian bio-fluid. *Anal. Chim. Acta* **559**, 15–24. (doi:10.1016/j.aca.2005.11.046)
29. Olivares ML, Vera-Candioti L, Berli CLA. 2009 The EOF of polymer solutions. *Electrophoresis* **30**, 921–929. (doi:10.1002/elps.200800578)
30. Zhao C, Yang C. 2011 Electro-osmotic mobility of non-Newtonian fluids. *Biomicrofluidics* **5**, 014110. (doi:10.1063/1.3571278)
31. Zhao C, Yang C. 2013 Electrokinetics of non-Newtonian fluids: a review. *Adv. Colloid Interface Sci.* **201–202**, 94–108. (doi:10.1016/j.cis.2013.09.001)
32. Owens RG. 2006 A new microstructure-based constitutive model for human blood. *J. Nonnewton. Fluid Mech.* **140**, 57–70. (doi:10.1016/j.jnnfm.2006.01.015)
33. Moyers-Gonzalez M, Owens RG, Fang J. 2008 A non-homogeneous constitutive model for human blood. Part 1. Model derivation and steady flow. *J. Fluid Mech.* **617**, 327. (doi:10.1017/S002211200800428X)
34. Vissink A, Waterman HA, Gravenmade EJ, Panders AK, Vermey A. 1984 Rheological properties of saliva substitutes containing mucin, carboxymethylcellulose or polyethylenoxide. *J. Oral Pathol. Med.* **13**, 22–28. (doi:10.1111/j.1600-0714.1984.tb01397.x)
35. Fam H, Bryant JT, Kontopoulou M. 2007 Rheological properties of synovial fluids. *Biorheology* **44**, 59–74.
36. Silva AF, Alves MA, Oliveira MSN. 2017 Rheological behaviour of vitreous humour. *Rheol. Acta* **56**, 377–386. (doi:10.1007/s00397-017-0997-0)
37. Afonso AM, Alves MA, Pinho FT. 2009 Analytical solution of mixed electro-osmotic/pressure driven flows of viscoelastic fluids in microchannels. *J. Nonnewton. Fluid Mech.* **159**, 50–63. (doi:10.1016/j.jnnfm.2009.01.006)
38. Ghosh U, Chakraborty S. 2015 Electroosmosis of viscoelastic fluids over charge modulated surfaces in narrow confinements. *Phys. Fluids* **27**, 062004. (doi:10.1063/1.4922585)
39. Mukherjee S, Goswami P, Dhar J, Dasgupta S, Chakraborty S. 2017 Ion-size dependent electroosmosis of viscoelastic fluids in microfluidic channels with interfacial slip. *Phys. Fluids* **29**, 72002. (doi:10.1063/1.4990841)
40. Ferrás LL, Afonso AM, Alves MA, Nóbrega JM, Pinho FT. 2016 Electro-osmotic and pressure-driven flow of viscoelastic fluids in microchannels: analytical and semi-analytical solutions. *Phys. Fluids* **28**, 093102. (doi:10.1063/1.4962357)
41. Mukherjee S, Das SS, Dhar J, Chakraborty S, DasGupta S. 2017 Electroosmosis of viscoelastic fluids: role of wall depletion layer. *Langmuir* **33**, 12 046–12 055. (doi:10.1021/acs.langmuir.7b02895)
42. Dhar J, Jaggi P, Chakraborty S. 2016 Oscillatory regimes of capillary imbibition of viscoelastic fluids through concentric annulus. *RSC Adv.* **6**, 60 117–60 125. (doi:10.1039/C6RA05002F)
43. Haeberle S, Zengerle R. 2007 Microfluidic platforms for lab-on-a-chip applications. *Lab. Chip* **7**, 1094–1110. (doi:10.1039/B706364B)
44. Mark D, Haeberle S, Roth G, von Stetten F, Zengerle R. 2010 Microfluidic lab-on-a-chip platforms: requirements, characteristics and applications. *Chem. Soc. Rev.* **39**, 1153. (doi:10.1039/B820557B)
45. Brust M, Schaefer C, Doerr R, Pan L, Garcia M, Arratia PE, Wagner C. 2013 Rheology of human blood plasmaâĂŤ: viscoelastic versus newtonian behavior. *Phys. Rev. Lett.* **78305**, 6–10. (doi:10.1103/PhysRevLett.110.078305)
46. Das T, Chakraborty S. 2013 Perspective: flicking with flow: can microfluidics revolutionize the cancer research? *Biomicrofluidics* **7**, 11811. (doi:10.1063/1.4789750)
47. Ohno K, Tachikawa K, Manz A. 2008 Microfluidics: applications for analytical purposes in chemistry and biochemistry. *Electrophoresis* **29**, 4443–4453. (doi:10.1002/elps.200800121)

Downloaded from https://royalsocietypublishing.org/ on 30 January 2023

48. Becker H, Gärtner C. 2000 Polymer microfabrication methods for microfluidic analytical applications. *Electrophoresis* **21**, 12–26. (doi:10.1002/(SICI)1522-2683(20000101)21:1<12::AID-ELPS12>3.0.CO;2-7)
49. Ziaie B, Baldi A, Lei M, Gu Y, Siegel R. 2004 Hard and soft micromachining for BioMEMS: review of techniques and examples of applications in microfluidics and drug delivery. *Adv. Drug Deliv. Rev.* **56**, 145–172. (doi:10.1016/j.addr.2003.09.001)
50. Chakraborty R, Dey R, Chakraborty S. 2013 Thermal characteristics of electromagnetohydrodynamic flows in narrow channels with viscous dissipation and Joule heating under constant wall heat flux. *Int. J. Heat Mass Transf.* **67**, 1151–1162. (doi:10.1016/j.ijheatmasstransfer.2013.08.099)
51. Majumder S, Dhar J, Chakraborty S. 2015 Resolving anomalies in predicting electrokinetic energy conversion efficiencies of nanofluidic devices. *Sci. Rep.* **5**, 14725. (doi:10.1038/srep14725)
52. Das S, Das T, Chakraborty S. 2006 Analytical solutions for the rate of DNA hybridization in a microchannel in the presence of pressure-driven and electroosmotic flows. *Sens. Actuators B Chem.* **114**, 957–963. (doi:10.1016/j.snb.2005.08.012)
53. Das S, Chakraborty S. 2011 Steric-effect-induced enhancement of electrical-double-layer overlapping phenomena. *Phys. Rev. E* **84**, 12501. (doi:10.1103/PhysRevE.84.012501)
54. Ajdari A. 1995 Electro-osmosis on inhomogeneously charged surfaces. *Phys. Rev. Lett.* **75**, 755–758. (doi:10.1103/PhysRevLett.75.755)
55. Ajdari A. 1996 Generation of transverse fluid currents and forces by an electric field: electro-osmosis on charge-modulated and undulated surfaces. *Phys. Rev. E* **53**, 4996–5005. (doi:10.1103/PhysRevE.53.4996)
56. Mandal S, Ghosh U, Bandopadhyay A, Chakraborty S. 2015 Electro-osmosis of superimposed fluids in the presence of modulated charged surfaces in narrow confinements. *J. Fluid Mech.* **776**, 390–429. (doi:10.1017/jfm.2015.333)
57. Ghosh U, Chakraborty S. 2012 Patterned-wettability-induced alteration of electro-osmosis over charge-modulated surfaces in narrow confinements. *Phys. Rev. E* **85**, 1–13. (doi:10.1103/PhysRevE.85.046304)
58. Ng WY, Goh S, Lam YC, Yang C, Rodríguez I. 2009 DC-biased AC-electroosmotic and AC-electrothermal flow mixing in microchannels. *Lab. Chip* **9**, 802–809. (doi:10.1039/B813639D)
59. Craster RV, Matar OK. 2005 Electrically induced pattern formation in thin leaky dielectric films. *Phys. Fluids* **17**, 032104. (doi:10.1063/1.1852459)
60. González A, Ramos A, Green NG, Castellanos A, Morgan H. 2000 Fluid flow induced by nonuniform AC electric fields in electrolytes on microelectrodes. II. A linear double-layer analysis. *Phys. Rev. E* **61**, 4019–4028. (doi:10.1103/PhysRevE.61.4019)
61. Chakraborty S. 2006 Augmentation of peristaltic microflows through electro-osmotic mechanisms. *J. Phys. D: Appl. Phys.* **39**, 5356. (doi:10.1088/0022-3727/39/24/037)
62. Chakraborty S, Srivastava AK. 2007 Generalized model for time periodic electroosmotic flows with overlapping electrical double layers. *Langmuir* **23**, 12 421–12 428. (doi:10.1021/la702109c)
63. Chakraborty S, Ray S. 2008 Mass flow-rate control through time periodic electro-osmotic flows in circular microchannels. *Phys. Fluids* **20**, 083602. (doi:10.1063/1.2949306)
64. Squires TM, Bazant MZ. 2004 Induced-charge electro-osmosis. *J. Fluid Mech.* **509**, 217–252. (doi:10.1017/S0022112004009309)
65. Garcia AL, Ista LK, Petsev DN, O'Brien MJ, Bisong P, Mammoli AA, Brueck SRJ, López GP. 2005 Electrokinetic molecular separation in nanoscale fluidic channels. *Lab. Chip* **5**, 1271–1276. (doi:10.1039/B503914B)
66. Ghosal S. 2004 Fluid mechanics of electroosmotic flow and its effect on band broadening in capillary electrophoresis. *Electrophoresis* **25**, 214–228. (doi:10.1002/elps.200305745)
67. Bandopadhyay A, Chakraborty S. 2012 Giant augmentations in electro-hydro-dynamic energy conversion efficiencies of nanofluidic devices using viscoelastic fluids. *Appl. Phys. Lett.* **101**, 043905. (doi:10.1063/1.4739429)
68. Nguyen T, Xie Y, de Vreede LJ, van den Berg A, Eijkel JCT. 2013 Highly enhanced energy conversion from the streaming current by polymer addition. *Lab. Chip* **13**, 3210. (doi:10.1039/C3LC41232F)
69. Chen CH, Lin H, Lele SK, Santiago JG. 2005 Convective and absolute electrokinetic instability with conductivity gradients. *J. Fluid Mech.* **524**, 263–303. (doi:10.1017/S0022112004002381)
70. Melcher JR. 1967 Traveling-wave bulk electroconvection induced across a temperature gradient. *Phys. Fluids* **10**, 1178. (doi:10.1063/1.1762260)

Downloaded from https://royalsocietypublishing.org/ on 30 January 2023

71. Ghonge T, Chakraborty J, Dey R, Chakraborty S. 2013 Electrohydrodynamics within the electrical double layer in the presence of finite temperature gradients. *Phys. Rev. E* **88**, 053020. (doi:10.1103/PhysRevE.88.053020)
72. Das S, Das T, Chakraborty S. 2006 Modeling of coupled momentum, heat and solute transport during DNA hybridization in a microchannel in the presence of electro-osmotic effects and axial pressure gradients. *Microfluid. Nanofluidics* **2**, 37–49. (doi:10.1007/s10404-005-0052-9)
73. Goswami P, Chakraborty S. 2010 Energy transfer through streaming effects in time-periodic pressure-driven nanochannel flows with interfacial slip. *Langmuir* **26**, 581–590. (doi:10.1021/la901209a)
74. Dey R, Chakraborty D, Chakraborty S. 2010 Analytical solution for thermally fully developed combined electroosmotic and pressure-driven flows in narrow confinements with thick electrical double layers. *J. Heat Transfer* **133**, 024503. (doi:10.1115/1.4002607)
75. Ghosal S. 2003 The effect of wall interactions in capillary-zone electrophoresis. *J. Fluid Mech.* **491**, 285–300. (doi:10.1017/S0022112003005330)
76. Datta S, Ghosal S. 2008 Dispersion due to wall interactions in microfluidic separation systems. *Phys. Fluids* **20**, 012103. (doi:10.1063/1.2828098)
77. Datta S, Ghosal S. 2009 Characterizing dispersion in microfluidic channels. *Lab. Chip* **9**, 2537–2550. (doi:10.1039/b822948c)
78. Paul S, Ng CO. 2012 Dispersion in electroosmotic flow generated by oscillatory electric field interacting with oscillatory wall potentials. *Microfluid. Nanofluidics* **12**, 237–256. (doi:10.1007/s10404-011-0868-4)
79. Ng CO, Zhou Q. 2012 Dispersion due to electroosmotic flow in a circular microchannel with slowly varying wall potential and hydrodynamic slippage. *Phys. Fluids* **24**, 112002. (doi:10.1063/1.4766598)
80. Das S, Chakraborty S. 2010 Effect of conductivity variations within the electric double layer on the streaming potential estimation in narrow fluidic confinements. *Langmuir* **26**, 11 589–11 596. (doi:10.1021/la1009237)
81. Das S, Chakraborty S, Mitra SK. 2012 Redefining electrical double layer thickness in narrow confinements: effect of solvent polarization. *Phys. Rev. E* **85**, 051508. (doi:10.1103/PhysRevE.85.051508)
82. Bandopadhyay A, Chakraborty S. 2011 Steric-effect induced alterations in streaming potential and energy transfer efficiency of non-Newtonian fluids in narrow confinements. *Langmuir* **27**, 12 243–12 252. (doi:10.1021/la202273e)
83. Sánchez S, Méndez F, Martínez-Suástegui L, Bautista O. 2012 Asymptotic analysis for the conjugate heat transfer problem in an electro-osmotic flow with temperature-dependent properties in a capillary. *Int. J. Heat Mass Transf.* **55**, 8163–8171. (doi:10.1016/j.ijheatmasstransfer.2012.08.027)
84. Bazant MZ, Thornton K, Ajdari A. 2004 Diffuse-charge dynamics in electrochemical systems. *Phys. Rev. E* **70**, 21506. (doi:10.1103/PhysRevE.70.021506)
85. Thien NP, Tanner RI. 1977 A new constitutive equation derived from network theory. *J. Nonnewton. Fluid Mech.* **2**, 353–365. (doi:10.1016/0377-0257(77)80021-9)
86. Bautista O, Sánchez S, Arcos JC, Méndez F. 2013 Lubrication theory for electro-osmotic flow in a slit microchannel with the Phan-Thien and Tanner model. *J. Fluid Mech.* **722**, 496–532. (doi:10.1017/jfm.2013.107)
87. Venditti R, Xuan X, Li D. 2006 Experimental characterization of the temperature dependence of zeta potential and its effect on electroosmotic flow velocity in microchannels. *Microfluid. Nanofluidics* **2**, 493–499. (doi:10.1007/s10404-006-0100-0)
88. Xuan X, Sinton D, Li D. 2004 Thermal end effects on electroosmotic flow in a capillary. *Int. J. Heat Mass Transf.* **47**, 3145–3157. (doi:10.1016/j.ijheatmasstransfer.2004.02.023)
89. Huang KD, Yang RJ. 2006 Numerical modeling of the Joule heating effect on electrokinetic flow focusing. *Electrophoresis* **27**, 1957–1966. (doi:10.1002/elps.200500721)